

# OPTIMIZATION OF VIBRATION TRANSMISSION SYSTEM BASED ON IMPLICIT PARAMETRIC MODELING OF SUGARCANE HARVESTER FRAME

## 基于机架隐式参数化建模的蔗秆切割损伤优化

Biao ZHANG<sup>1,2\*</sup>, Weimin SHEN<sup>1)</sup>, Dan PAN<sup>1)</sup>

<sup>1)</sup>College of Mechanical Engineering, Guangxi University, Nanning, 530004, China;

<sup>2)</sup>Guangxi Key Laboratory of Environmental Pollution Control and Ecological Restoration Technology, Nanning 530007, China

\* Correspondence: bzhang@gxu.edu.cn

DOI: <https://doi.org/10.35633/inmateh-75-60>

**Keywords:** sugarcane harvester, cutting damage, vibration transmission, dynamic optimization, parametric modeling

### ABSTRACT

The hilly terrain where sugarcane harvesters travel, the harvest object of rough and tough stalks, and the perennial cultivation property are all different from those of other straw crops. In order to reduce the cutting damage of cane stalks caused by complex excitation in field conditions, a method for optimizing dynamic characteristics of vibration transmission system based on implicit parametric modeling of harvester frame was proposed. First, the impact damage effect of the cutter on the cut section of stalk was analyzed by high-speed images. Accordingly, the cutter amplitude RMS and impact velocity ( $V_I$ ) were proposed as parameters to characterize the damage inducibility. Subsequently, a 5-DOF dynamic model of the whole machine was established covering 21 dynamic parameters. With the measured excitation of road spectrum, cane cutting force and engine, the virtual prototype simulation showed that the frame stiffness was the most sensitive to vibration response. Through topology optimization and implicit parametric modeling of such load-bearing frame, a high-rigidity design was derived to improve the vibration transmission characteristics. Comparison of testing results before and after frame optimization illustrated that the bending stiffness and torsional stiffness were increased by 1.95% and 2.84% respectively, and the RMS of operating frequency-response functions with road and engine as path sources were decreased by 21.7% and 27.2% respectively. As a result, the output amplitude RMS and impact velocity  $V_I$  were reduced by 35.9% and 5.9% respectively, implying corresponding improvements in the cutting quality of cane stalks. This study provided a reference for the development of harvester dynamic systems based on harvesting quality optimization.

### 摘要

甘蔗收获机的丘陵行进地形、粗韧茎秆割收对象及其宿根种植性状与其它秸秆作物条件不同。为降低蔗地工况复杂激励所致的蔗秆切割损伤，本文提出了一种基于机架隐式参数化建模对蔗秆切割损伤进行优化的方法。首先利用高速摄像图像剖析了刀盘-茎秆互作的冲击损伤效应。据此提出了采用刀盘振幅 RMS 和冲速 ( $V_I$ ) 作为诱损性表征参量。随后，基于实测路谱建立了整机 5 自由度动力学模型，解析发现机架刚度对动力响应的敏感性最大。进而筛选出可映射机架承载式结构特征的 21 个设计变量，从而建立其隐式参数化模型，并通过拓扑优化衍生出机架高刚性的优化设计。优化前后的对比测试结果表明，其弯曲、扭转刚度分别提高 1.95% 和 2.84%，以路面、发动机为路径源的传振频响函数 RMS 各降低 21.7% 和 27.2%。综合引起致损振幅 RMS 和冲速  $V_I$  降低了 35.9% 及 5.9%，意味着蔗秆切割质量获得相应的改进。该研究可为收获机械的动力学系统开发及收割质量优化提供参考。

### INTRODUCTION

Sugarcane is a perennial crop whose post-harvest residual stumps germinate, emerge and grow up at cane nodes under suitable environmental conditions (Liu *et al.*, 2018). At present, the planting area of ratoon sugarcane accounts for more than 70% of the total sugarcane area (Yang *et al.*, 2021; Wu *et al.*, 2022), so the germination rate directly affects the yield and efficiency of the next year. Since the main sugarcane-producing regions, such as Guangxi and Yunnan Provinces, are widely distributed across the hilly areas of South China, sugarcane harvesters often operate on uneven ridge-furrow terrain. Furthermore, due to the thick and highly fibrous nature of cane stalks, harvesters typically adopt a low-position cutting method, inserting the cutter deep into the soil to improve cutting efficiency (Mo *et al.*, 2013). The above compound working conditions are obviously different from the harvesting conditions of other straw crops such as corn and cotton, and have a

significant impact and instability on the key high-speed rotary cutter (Zou *et al.*, 2018). In the coupled environment of sugarcane fields, harvesters, and sugarcane plants, the harvester experiences vertical oscillations as it moves along uneven terrain. Influenced by multiple excitation sources, the cutting tool undergoes severe vibration, which can easily lead to damage of the budding nodes on the remaining cane stumps. These cutting quality issues significantly hinder the germination of ratoon sugarcane and have become a major bottleneck limiting sustainable and efficient sugarcane cultivation cycles.

So far, from the perspective of factors contributing to stalk cutting damage, Gupta *et al.* (1992), Razavi *et al.* (2010), and Wang *et al.* (2019) have experimentally analyzed the effects of structural and operational parameters - such as disc cutter configuration, blade layout, and rotational speed - on sugarcane harvest damage. Kroes *et al.* (1995) developed a model which described the base-cutter kinematics of the dual base-cutter sugarcane harvester. By using the model, the maximum permissible velocity ratio (forward speed/disc rotational speed) was calculated, which improved the cutting quality. Silva *et al.* (2008) evaluated the sugarcane root damage degree caused by cutting height differences through experiments. Peloso *et al.* (2021) studied effects of the cutter rotating speed and the sugarcane harvester moving speed on the cutting quality of sugarcane harvesters. Li *et al.* (2017) and Ma *et al.* (2006) analyzed the role relationship of system design elements on the cracking damage rate from perspectives of blade edge angle, travel speed and embedded depth. However, the cutting action of the blade is characterized by high speed, strong intermittent, short duration and invisible contact interface, making it difficult to use visual testing methods to effectively and accurately monitor the cutting process and damage evolution. In this regard, Liu *et al.* (2007) used high-speed cameras to experimentally test the splitting caused by the smooth blade cutting, and simulated the damage behavior of sugarcane under different load forms of tension, compression, bending and torsion (Liu *et al.*, 2007). Kroes *et al.* (1996) measured and predicted the force, energy, bending strength and splitting of sugarcane stalk during impact cutting. Mello *et al.* (2001) and Momin *et al.* (2017) studied the effects of the angle and serrated blades on the damage, force and energy and verified them by indoor high-speed camera and field test. In order to intuitively reveal the dynamic relationship and local structural characteristics of their interactions. Lv *et al.* (2008) and Yang *et al.* (2017) respectively established digital models of stem-plants based on structure-function, and simulated the damage process in the cutting motion by finite element method (FEM). The factors affecting the cutting state and extrusion of the cane head, as well as their interaction on the damage process, were quantitatively studied through virtual experiments.

Based on previous studies (Zhou *et al.*, 2017; Fan *et al.*, 2012), it has been confirmed that the cutting damage of sugarcane is significantly correlated with the amplitude of cutter, and the damage degree deepens as the amplitude increases. The vibration response output of the cutter is actually related to the imbalance caused by its own manufacturing and installation errors. It also interacts with the alternating loads on the whole vehicle generated by field road spectrum, engine, cutting force and other excitation sources. It itself is closely related to the dynamic characteristics of the vibration transmission system consisting of the frame, power gearbox, hydraulic lifting device, tires and other components. The system dynamics parameters involved include component mass and stiffness, connection stiffness and damping, power mounting position, etc. Therefore, from the perspective of a multi-source and multi-component coupled system, an in-depth analysis of the dynamic characteristics of such vibration transfer system from the excitation source to the response point is conducive to establishing the influence relationship between dynamic parameters and responses (Hou *et al.*, 2021; Xu *et al.*, 2017). Thus, the insensitive factors can be eliminated, the dynamical parameters of the dominant factors can be improved, and the characteristics of components can be optimized in terms of modal, lightweight and so on. Further, on the basis of considering the dynamic response, the forward design of the whole machine is guided to achieve the purpose of improving the sugarcane cutting quality.

Regarding the problem of cutting damage caused by vibration, this paper first analyzed the characteristics of excitation sources experienced by the sugarcane harvester under working conditions, and improved the response vibration evaluation from the perspective of cutting damage mechanism. Then, a dynamic analytical model of the vibration transmission system under action of multiple vibration sources was established. On this basis, a rigid-flexible coupling virtual prototype model was established to solve the nonlinear response, and the influence and correlation of multiple dynamic parameters on the response were analyzed. After screening, implicit parametric modeling and topology optimization design were carried out on the frame. Finally, the system dynamic characteristics were experimentally tested using the frequency-response function of the frame structure and the vibration characteristics of the response target to estimate the improved degree in sugarcane cutting damage.

## MATERIALS AND METHODS

### Principle of sugarcane cutting damage

#### Analysis of excitation Sources

##### Observation of damage morphology

During the operation of sugarcane harvester, the high-speed rotating cutterhead is subjected to various excitation in the process of cutting and conveying sugarcane, resulting in obvious axial vibration. Through observation, this vibration effect is usually accompanied by the splitting damage effect of ratoon cane stumps, as shown in Figure 1. The main forms of damage are penetrating tears and splitting notches along longitudinal stem-nodes. It is inferred that such damage is mainly attributed to the action of squeezing impact force when the blade comes into contact with cane material. Therefore, it is necessary to trace the sources of axial vibration of the cutter from the entire harvesting machine, including the forced vibration caused by field road spectrum, the second-order unbalanced inertial force of engine, and the self-excited vibration caused by sugarcane cutting.

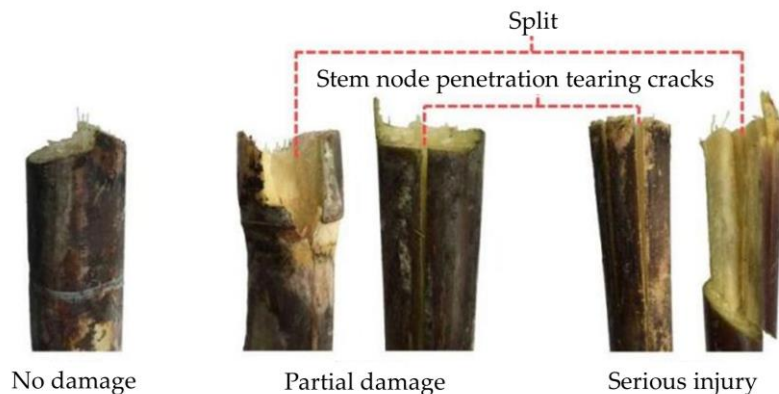


Fig. 1 - Cutting damage of sugarcane stubble

##### Measurement of field road spectrum

Using a portable data acquisition front end and PCB three-axis acceleration sensors, under a constant speed condition of  $0.8 \text{ m}\cdot\text{s}^{-1}$ , the Z-direction acceleration signal of a typical sugarcane field in the hilly area of Guangxi was collected as a road spectrum. The timing signal was then denoised through the MATLAB wavelet packet, and its amplitude-frequency curve was obtained using Fourier transform, as shown in Figure 2. It can be seen that road excitation is a low-frequency and high-amplitude displacement load, with frequencies concentrated within 10 Hz and the peak value appearing at 2.5 Hz.

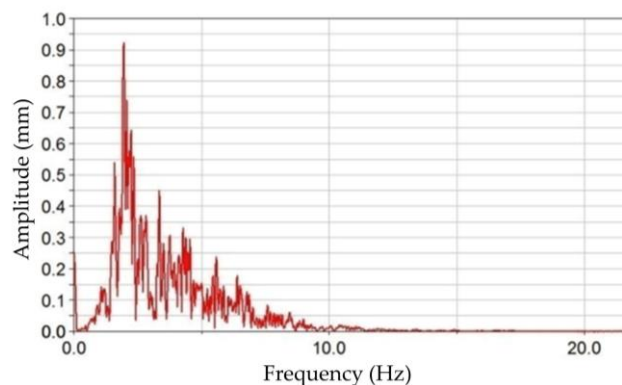


Fig. 2 - Amplitude-frequency curve of hilly field road spectrum

##### Calculation of engine excitation force

For the second-order reciprocating inertia force caused by the eccentricity of the engine cylinder, the calculation formula is as follows (Gu *et al.*, 2013):

$$F_{2nd} = 4 \cdot m_o \cdot r \cdot \omega^2 \left( \lambda + \frac{3}{2} \lambda^3 \psi^2 \right) \cos 2\alpha \quad (1)$$

where:  $m_o$  is the cylinder weight, kg;  $r$  is the crankshaft crank radius, m;  $\omega$  is the angular velocity, rad/s;  $\lambda$  is the ratio of connecting rod;  $\psi$  is the eccentricity;  $\alpha$  is the crank angle. In addition, the vertical vibration frequency of the engine follows:

$$f = \frac{Qn}{60} \tag{2}$$

where: Q is the proportional coefficient, which takes a value of 2 under the second-order inertia force; n is the engine speed, r/min.

Referring to the recorded cylinder parameters and the engine speed range of 1500~2000 rpm under working conditions (Zhou et al., 2018), it can be calculated that the excitation force from the engine is approximately 2493 N and the f is about 50~66.7 Hz.

Measurement of sugarcane cutting force

During the experimental sugarcane cutting process, a quartz three-phase dynamometer was used to collect the axial cutting force at a sampling frequency of 20 kHz. The data after using Matlab wavelet package to denoise the time-series signal is shown in Figure 3. At the same time, in order to understand the instantaneous cutting process of cane, an industrial camera was employed to focus on the cutting position of the stalk and record the frame images at four sequential cutting moments of the blade during cutting off a single cane, as shown in Fig. 4.

Based on Figure 3 and Figure 4, it can be seen that there were four equidistant peaks in the cutting force signal, indicating that the rotating blades of the cutter cut off a single cane after four repeated cuts. This was consistent with the results of high-speed photographic images. By calculating the sampling frequency and the number of sampling points, it was found that the cutting action time of single blade was extremely short, approximately 0.0023 s, and thus the cutting excitation frequency was about 434.8 Hz, which was a high-frequency self-excited vibration.

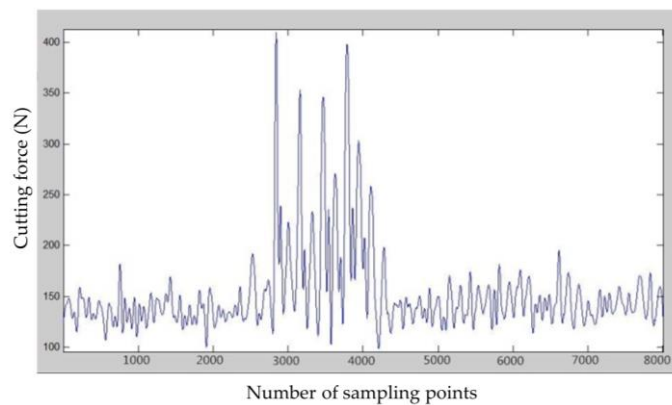
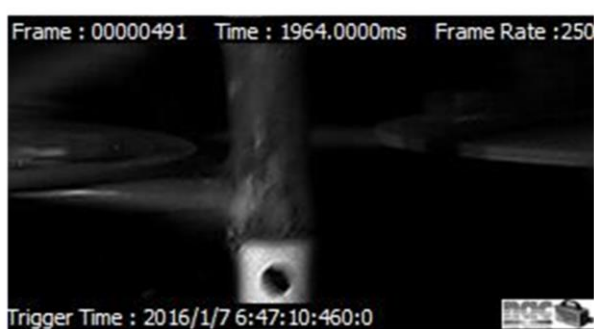


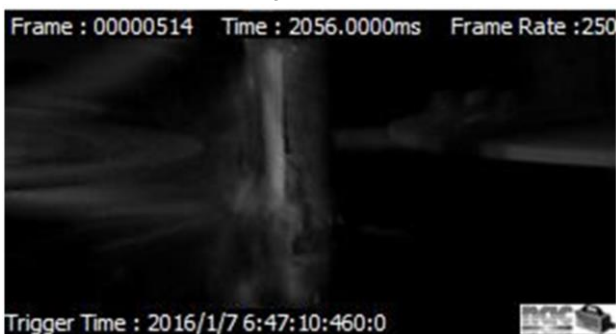
Fig. 3 - Cutting force pulse signal for cutting off single sugarcane



(a) Image at 1964 ms



(b) Image at 2008 ms



(c) Image at 2056 ms



(d) Image at 2100 ms

Fig. 4 - Sequential high-speed images of repeated cuts of a single stalk

### Vibration evaluation index based on sugarcane damage process

Figure 5 shows the axial vibration of the working cutterhead sampled using a laser displacement sensor. Since the periodic displacement change of the cutter affects the cutting position of the stalk, the root mean square (RMS) of the amplitude was first used as the response index. In addition, within a single cutting duration of about 0.0023 s, a positive pressure ( $F_N$ ) of about 246 N (taken from the average of the peak values in Figure 3) acted on the sugarcane cross-section, so the impulse ( $I$ ) generated at the instant of cutting was calculated to be about 0.57 N·s, causing the cane material to crack. Further, since there was a certain interval of about 0.013 s between two consecutive cuts, as the cutting depth gradually increased, the second to fourth cuts can produce a certain bending moment ( $M$ ), causing cracks to continue to expand:

$$M = F_N \cdot \Delta s \cdot i \quad (3)$$

where  $\Delta s$  is the feeding depth for a single cut, which is related to the harvester driving speed;  $i=2, 3, 4$ .

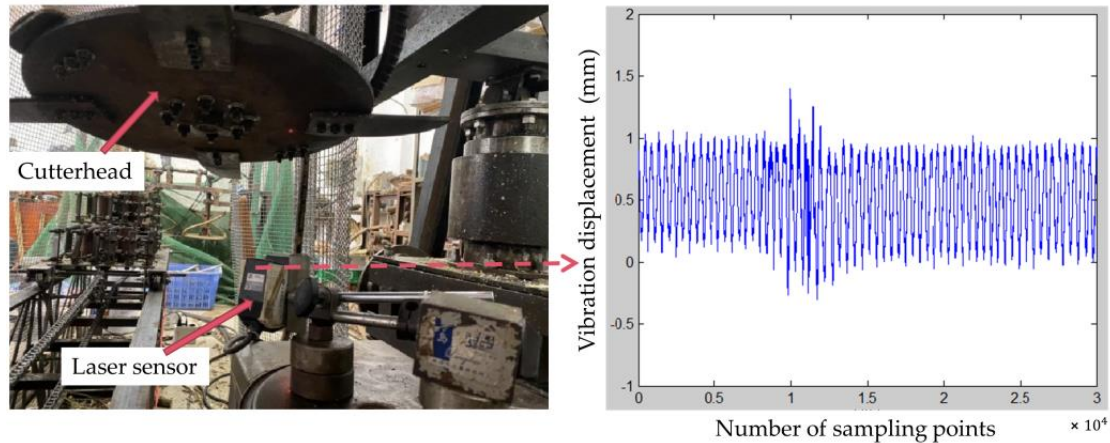


**Fig. 5 – Cutter vibration signal measurement**

Based on the above analysis, it can be known that the joint action of  $F_N$ ,  $I$  and  $M$  lead to the damage of sugarcane nodes. Considering the spatial-temporal observation of instantaneous cutting, the single cutting time ( $\Delta t$ ) of the blade is close to zero, and the corresponding axial relative displacement ( $\Delta u$ ) is formed. Therefore, the impact velocity ( $V_I$ ) can be defined to characterize the impact strength of the cutter on the section:

$$V_I = \lim_{\Delta t \rightarrow 0} \frac{\Delta u}{\Delta t} \quad (4)$$

In summary, based on the analysis of the damage mechanism of sugarcane cutting, the indicators of cutter amplitude *RMS* and impact velocity were proposed, thus forming a comprehensive response evaluation covering macroscopic vibration energy and local impact intensity. It was helpful to comprehensively evaluate the relationship between the cutter vibration responses and cutting damage.

### **Dynamic modeling of vibration transmission system**

#### *Dynamic model*

The main vibration excitation devices installed on the frame include front guide wheels, rear drive wheels, cutting system and engine. Therefore, it is necessary to study the impact of the combined effects of ground roughness, engine cycle excitation force and cutting force on the dynamic characteristics of the whole machine, especially reflected in the impact on cutter vibration. The sugarcane harvester was simplified as a mass-spring-damping system (Mo et al., 2022), in which the four wheels were simplified into spring coupled damping. The dynamic theoretical model established is shown in Figure 6 (a). Based on the Z-direction sensitivity to cutting damage, this model only considered the degrees of freedom (DOF) in the three directions of vertical vibration (along the Z direction), transverse torsional vibration (around the Y-axis) and longitudinal torsional vibration (around the X-axis). Thus, the model contains 5-DOF, which are the vertical displacement of frame centroid ( $X_1$ ), the rotation angle around X-axis ( $\theta_1$ ), the rotation angle around Y-axis ( $\theta_2$ ), and the vertical displacement of engine centroid ( $X_2$ ) as well as the vertical displacement of cutting system ( $X_3$ ).

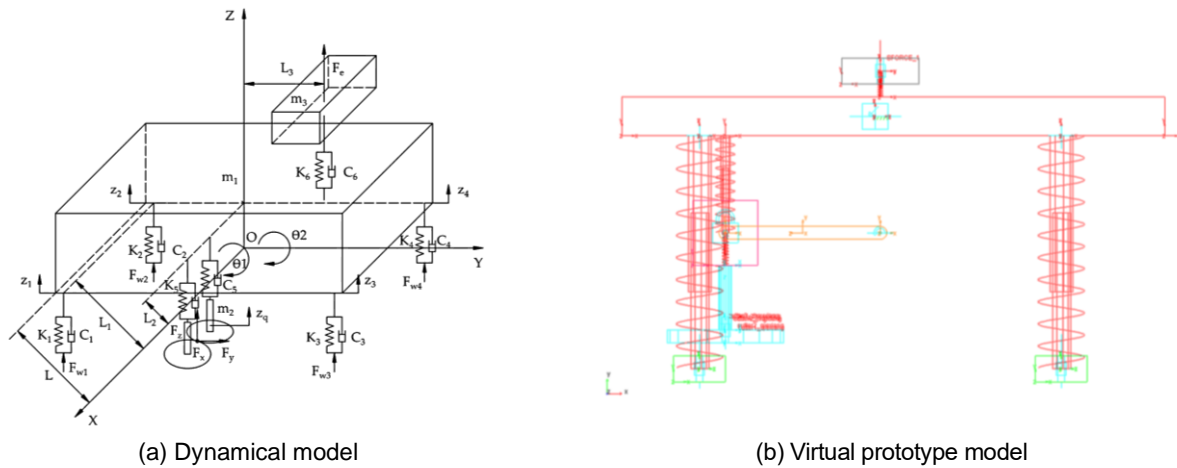


Fig. 6 - The frame model

Note:  $m_1$ ,  $m_2$  and  $m_3$  are masses of frame, power gearbox and engine, kg;  $K$  is stiffness, N/m;  $C$  is damping, N/(m/s);  $K_1$ ,  $K_2$ ,  $C_1$  and  $C_2$  are stiffness and damping of the front wheels;  $K_3$ ,  $K_4$ ,  $C_3$  and  $C_4$  are stiffness and damping of the rear wheels;  $K_5$  and  $C_5$  are stiffness and damping of the lifting hydraulic cylinder between gearbox and frame;  $K_6$  and  $C_6$  are stiffness and damping of the engine suspension;  $F_{w1} \sim F_{w4}$  are road spectrum excitation loads on four wheels;  $F_e$  is vertical excitation force from the engine, N;  $F_x$ ,  $F_y$  and  $F_z$  are respectively the radial, tangential and axial cutting force, N;  $L$  is half the length of frame, m;  $L_1$  is the distance from front wheel or rear wheel to frame centroid, m;  $L_2$  is the distance from gearbox to frame centroid, m;  $L_3$  is the distance from engine to frame centroid, m;  $z_i$  is the vertical displacement of each wheel, m;  $z_q$  is the vertical displacement of cutting system, m.

**Virtual prototyping simulation**

Since the analytical model is a complex multi-DOF nonlinear system, the ADAMS 2020 software was used to establish a virtual prototype simulation model to solve the correlation coefficients between the above 21 dynamic parameters and the cutter vibration response (Zhang et al., 2023; Han et al., 2022). As shown in Figure 6 (b), a total of 11 components were created. The frame and engine parts were flexibly processed and then assembled with other rigid body parts, to reflect their stiffness characteristics, i.e. elastic modulus  $E_1$  and  $E_2$  respectively. Moreover, the required constraints, including global Y-direction translation, rotations around Z-direction and X-direction, were applied. The measured field road spectrum excitation (Fig. 2), the measured cane cutting force (Fig. 3) and the engine excitation force, modeled as a sine wave, were applied as loads to simulate real driving conditions.

**Experimental testing of frame dynamic characteristics**

Modal testing

The experimental bench model of the sugarcane harvester is shown in Figure 7, which includes the key operating assemblies.

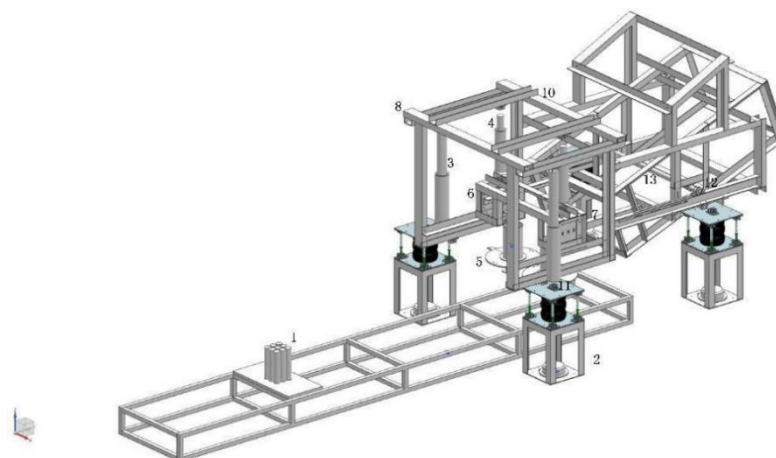


Fig. 7 - General assembly of the whole machine system

- 1- sugarcane clamping conveying device; 2- road spectrum exciter; 3- overall lifting hydraulic cylinder; 4- hydraulic cylinder for partial lifting of the cutting system; 5- cutter; 6- gearbox; 7- cantilever; 8- frame; 9- conveying rack; 10- motor for engine excitation; 11- exciter hinge; 12- logistics hinge; 13- pin shaft

The excitation devices involve mechanical road exciters, a triple-phase asynchronous motor, frequency converters and an infrared photoelectric speedometer for calibration. With these, low-frequency road excitation, engine excitation of 50 Hz and high-frequency cutting force excitation can be achieved in experiments. As the main rigid component that supports various parts of cane cutting system, the beam-structure frame bears the dynamic loads under working conditions. The purpose of modal analysis is to find the weak points of the frame under the excitation loads based on its natural vibration forms, so as to provide a reference for subsequent optimization.

The modal testing was performed using an LMS data acquisition system, PCB three-axis acceleration sensors, and an excitation hammer. With the single-point excitation and multi-point response method, the PCB sensors were arranged at 66 measuring points on the whole machine, as shown in Figure 8. In this way, constrained modal frequencies and vibration modes can thus be analyzed to search for locations of weak dynamic stiffness while avoiding frequency resonances.

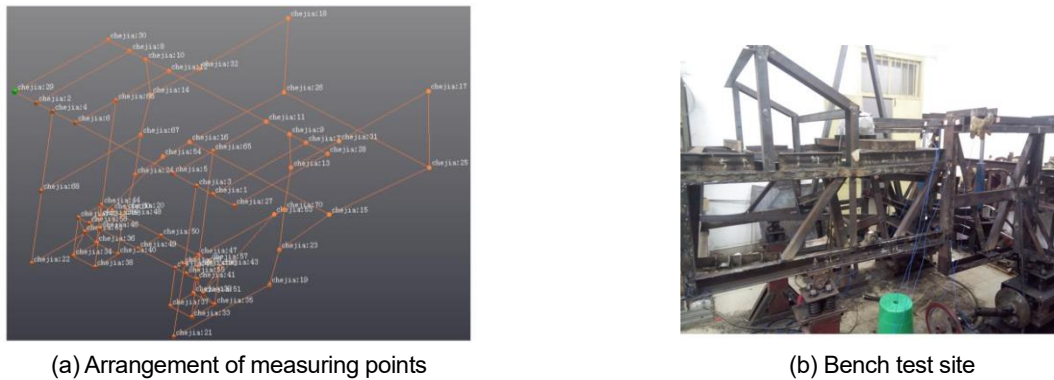


Fig. 8 - Modal Testing

Frequency-response function testing

Since the frame is the main transfer path from vibration sources to the cutter, it is necessary to test the vibration transfer function (VTF) before and after structural modifications. When the RMS of VTFs decreases and the peak frequency is far away from the excitation frequency, it means that the vibration isolation performance of the frame on the vibration transmission path is improved, and the response caused by the same excitation intensity is reduced. In addition, since the axial vibration of the cutter is most sensitive to the vertical vibration of the frame, the vertical VTF should be adopted.

With the road and engine vibration sources activated, a PCB acceleration sensor was arranged at the critical gearbox where the cutter was installed, as shown in Figure 9. Similarly, the LMS data acquisition system was employed to collect the response data of this target point of interest under multi-source vibration. Thus, the processed vertical frequency-response functions (FRF) from the two excitation sources to this response output location can be calculated as follows:

$$H(\omega) = \frac{t(\omega)}{f(\omega)} \tag{5}$$

where:

$t(\omega)$  is the frequency-related response at the target point, taking 0~100 Hz as the frequency analysis range;  $f(\omega)$  is the hammer excitation force. In addition, the real time-domain signal of the cutter displacement before and after the frame optimization was also tested using the Laser vibration testing system, and its amplitude RMS was used as an indicator to verify the final optimization effect.

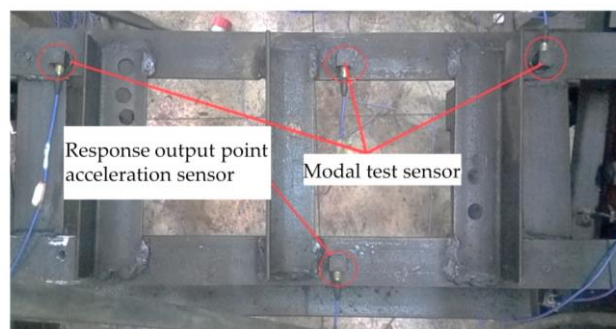


Fig. 9 - Response output signal acquisition

## Optimized Design of Frame Structure

### Multi-objective Topology Optimization

Considering the requirements of static Z-direction stiffness and dynamic vibration frequency, a comprehensive multi-objective optimization function combined compromise planning method with average frequency method was adopted for the frame structure (Liu *et al.*, 2022):

$$\min F = \left\{ \omega^2 \left( \frac{C(\rho) - C_{\min}}{C_{\max} - C_{\min}} \right)^2 + (1 - \omega)^2 \left( \frac{\Lambda_{\max} - \Lambda(\rho)}{\Lambda_{\max} - \Lambda_{\min}} \right)^2 \right\}^{1/2} \quad (6)$$

where:

$C(\rho)$  and  $\Lambda(\rho)$  are objective functions of flexibility and average frequency;  $\omega$  is the weight of flexibility. Thus, the optimal material distribution capable of comprehensively improving stiffness and dynamic frequency can be suggested in the design domain to guide the frame shape design.

Besides, in ANSYS 14.5 software, the beam elements in the non-optimized region were set to SOLID92 and the shell elements in the optimized region were set to SHELL93. Dynamic single-step load conditions were applied simultaneously with the simple harmonic forces of the field road and the engine on the frame. Then, taking  $\omega$  as 0.4, the iterative control of optimization objectives was implemented based on APDL language programming.

### Implicit parametric modeling

In order to solve the problem of steel specification selection of the main load-bearing beams in the frame structure, an implicit parameter-based modeling of the frame was carried out to further obtain a better beam structure design scheme in terms of inherent dynamic characteristics (Chen *et al.*, 2016). For the main force deformation forms of the beam, bending and torsion, its moment of inertia and polar moment of inertia depend on its cross-sectional shape and size. Hence, several stressed beams with large bending and torsion degrees were extracted based on the modal results, and their cross-sectional dimensions were used as parametric design variables ( $V_i$ ). The ANSYS command flow was actually employed to create these beams to be optimized. The beam element used Beam188, which was a two-node three-dimensional linear element suitable for linear, large-angle or large-strain nonlinear analysis of slender to medium-thick short beam structures. As a result, an implicit parameterized model of the frame containing material properties, solder joints, constraints and other information was obtained, as shown in Figure 10.

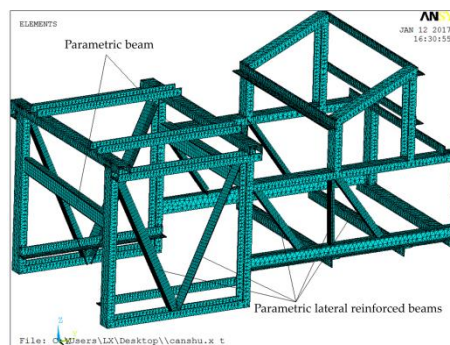


Fig. 10 – Implicit parametric model

Taking the reduction of the frame mass and moving the dangerous natural frequency out of the resonance frequency band as constraints, and aiming to increase the first to four-order natural frequencies as the goal, a mathematical model for beam section size optimization was established:

$$\begin{cases} \min F(V_i) = 1/f_{av} \\ s. t. \begin{cases} V_{i\min} \leq V_i \leq V_{i\max} \\ (50 - f_5) \cdot (66.7 - f_5) \geq 0 \\ m \leq m_o \end{cases} \end{cases} \quad (7)$$

where:

$f_{av}$  is the low-order average frequency, Hz;  $V_i$  is the  $i$ -th design variable,  $i=1,2...10$ ;  $f_5$  is the 5th-order dangerous resonance frequency, Hz;  $m_o$  is the initial mass of frame, kg. Based on the conditions, a parametric optimization design was carried out using a zero-order algorithm with a maximum number of iterations of 30 (Yan *et al.*, 2020).

**RESULTS**

**Correlation analysis of cutter vibration**

Under the joint action of road spectrum excitation, periodic excitation of engine and cane cutting pulse excitation, the simulated vibration response of the cutter is shown in Figure 11. It can be seen that the RMS of the cutter displacement response is 2.64 mm, and the RMS of the vibration velocity is 74.6 mm·s<sup>-1</sup>. The average displacement during a single cutting is 0.17 mm, which can produce an impulse on the cut surface. The average displacement during the interval between two cuts is 0.97 mm, which could cause obvious bending moments to promote crack expansion.

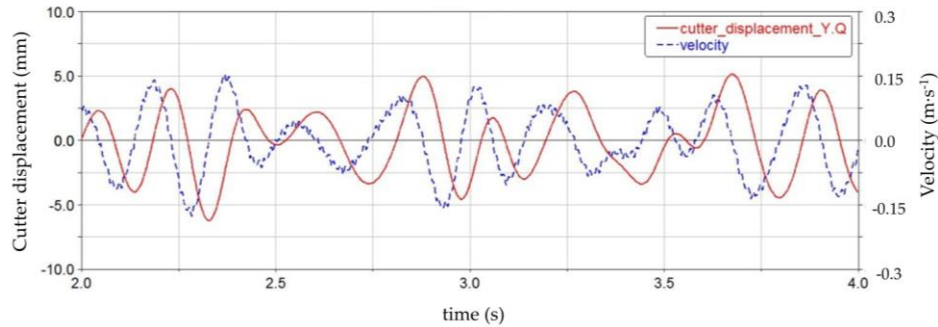


**Fig. 11 - Nonlinear response of vibration**

The correlation between dynamic parameters and cutter vibration was analyzed, and the results are shown in Table 1. It was found that the stiffness and mass ( $E_1$  &  $m_1$ ) of the frame had a higher impact on vibration, which was related to the fact that the frame structure accounted for the largest proportion and was the most widely distributed in the harvester. Therefore, the frame should be the main object of structural dynamics optimization where computing resources are concentrated.

**Table 1**

Correlation analysis results		
Dynamic parameters	Amplitude correlation	Impact velocity correlation
$m_1$	-0.073	0.134
$m_2$	0.022	-0.055
$K_1$	0.051	-0.020
$K_3$	-0.010	0.074
$K_5$	-0.016	0.019
$K_6$	0.009	-0.023
$L_1$	0.026	-0.055
$L_2$	0.006	-0.014
$L_3$	-0.008	0.013
$E_1$	0.168	-0.122
$E_2$	0.091	-0.027

**Analysis of frame dynamic characteristics**

The simulated and measured low-order frequency results below 50 Hz are shown in Table 2, and the corresponding vibration modes are shown in Figure 12. The errors between the finite element simulation results and the actual values are all less than 5%. Taking into account the errors in bench processing and assembly, it is believed that the accuracy requirements can be met. This suggests that further dynamic optimization can be carried out for the finite element model of frame. At the same time, it was found that the 5th-order natural frequency was close to the engine excitation frequency range, indicating that a dangerous resonance frequency currently existed.

**Table 2**

Comparison of modal results from finite element simulation and actual testing			
Order	Simulated frequency (Hz)	Tested frequency (Hz)	Description of vibration modes
1	21.1	20.5	X-direction oscillation
2	25.9	25.0	Z-direction oscillation
3	40.0	38.6	X-direction first-order torsion
4	47.6	45.3	Z-direction first-order bending
5	53.0	51.2	X-direction second-order torsion

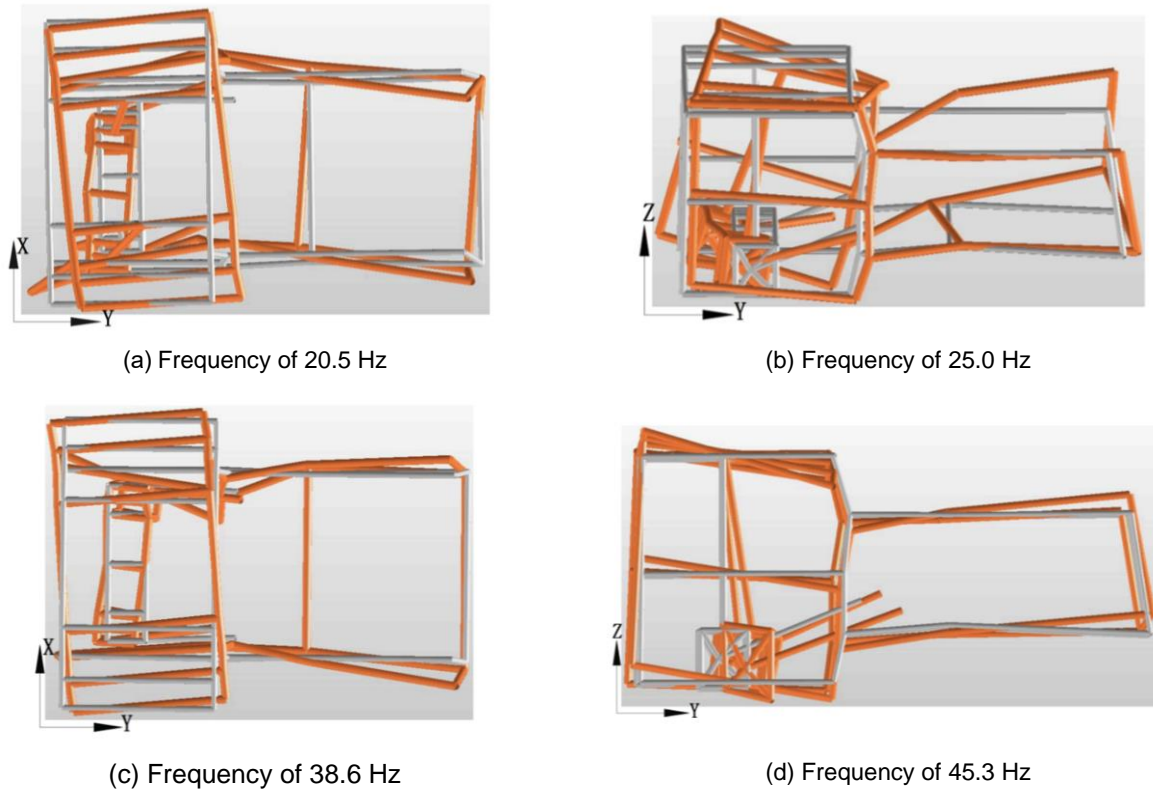


Fig. 12 - Vibration modes for modal testing

From the constrained modal results in Figure 12, the vibration modes and their frequencies were consistent with the finite element results. The combination of the four vibration modes showed that the dynamic stiffness of the frame was insufficient in the lateral and vertical directions, especially the open structure at the front end lead to severe lateral oscillations. Therefore, it was judged that the supporting structure located on the sides of the frame and the beam structures with right-angle bends were weak links and should be regarded as optimization focus.

**Analysis of frame optimization**

Figure 13(a) shows the density cloud diagram obtained by topology optimization of the frame under the condition of material removal rate of 50%. It has gradually evolved from the initial full-coverage plate-shell elements to a specific structural distribution composed of support beams. After extracting and simplifying the features of material-concentrated area, the reconstructed frame model is shown in Figure 13(b). The comparison results between the natural frequencies of the reconstructed model and the original values after topology optimization are shown in Table 3. The low-order frequencies have been increased by 17.91% to 86.37%, indicating that the dynamic characteristics have been further improved.

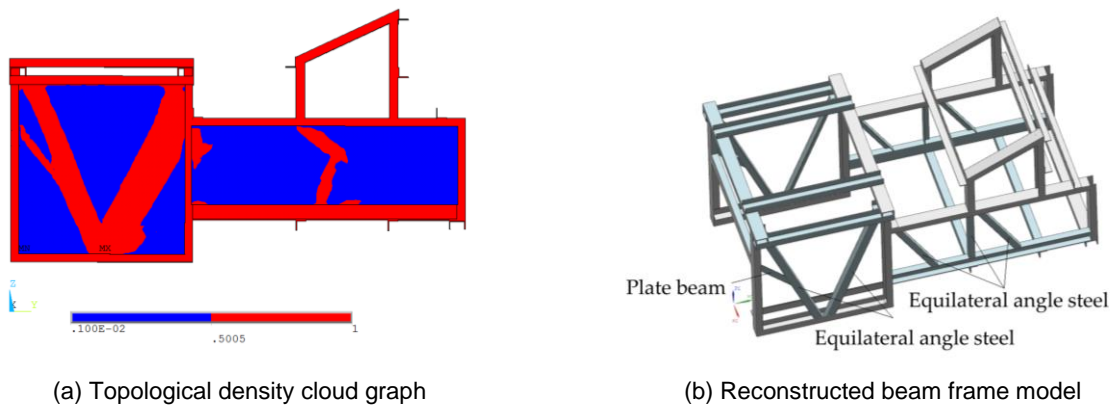


Fig. 13 - Multi-objective topology optimization results

Table 3

Comparison of natural frequencies before and after reconstruction

Natural frequency	Topology optimized	Reconstructed	Rate of change (%)
$f_1$ (Hz)	19.77	23.31	17.91
$f_2$ (Hz)	25.04	36.10	44.17
$f_3$ (Hz)	25.46	47.45	86.37
$f_4$ (Hz)	36.09	47.89	32.70

The initial values, constraints and parameter optimization results for parameterized variables and multi-objectives are shown in Table 4. Comparing the dynamic performance before and after optimization shows that without increasing the mass of the frame, the low-order frequencies of the frame were increased and the dangerous fifth-order natural frequency was moved out of the engine's resonance frequency band, achieving the expected optimization effect. Besides, the specification combination of steel dimensions for the main load-bearing beams was determined.

Table 4

Parameterized optimization results

Variables	Definition	Initial	Constraint	Optimized
$V_1$ (mm)	Front crossbeam channel steel width	80	50 ~120	85.3
$V_2$ (mm)	Front crossbeam channel steel height	43	35 ~55	48.9
$V_3$ (mm)	Front crossbeam channel steel thickness	5	4~6	4.3
$V_4$ (mm)	Middle crossbeam rectangular steel width	60	40~80	47.7
$V_5$ (mm)	Middle crossbeam rectangular steel height	90	70~120	70.8
$V_6$ (mm)	Middle crossbeam rectangular steel thickness	4	3~5	3.3
$V_7$ (mm)	Front side beam angle steel edge length	50	40~60	56.7
$V_8$ (mm)	Front side beam angle steel thickness	5	3~6	3.0
$V_9$ (mm)	Rear side beam angle steel edge length	40	30~50	46.2
$V_{10}$ (mm)	Rear side beam angle steel thickness	5	3~5	3.2
$m_1$ (kg)	Frame mass	195.7	$\leq 195.7$	195.5
$f_1$ (Hz)	1 <sup>st</sup> -order frequency	28.5		29.2
$f_2$ (Hz)	2 <sup>nd</sup> -order frequency	31.1		32.7
$f_3$ (Hz)	3 <sup>rd</sup> -order frequency	38.9		39.2
$f_4$ (Hz)	4 <sup>th</sup> -order frequency	49.1		49.9
$f_5$ (Hz)	5 <sup>th</sup> -order frequency	58.3	$\leq 50$ or $\geq 66.7$	66.9

Analysis of frequency-response characteristics

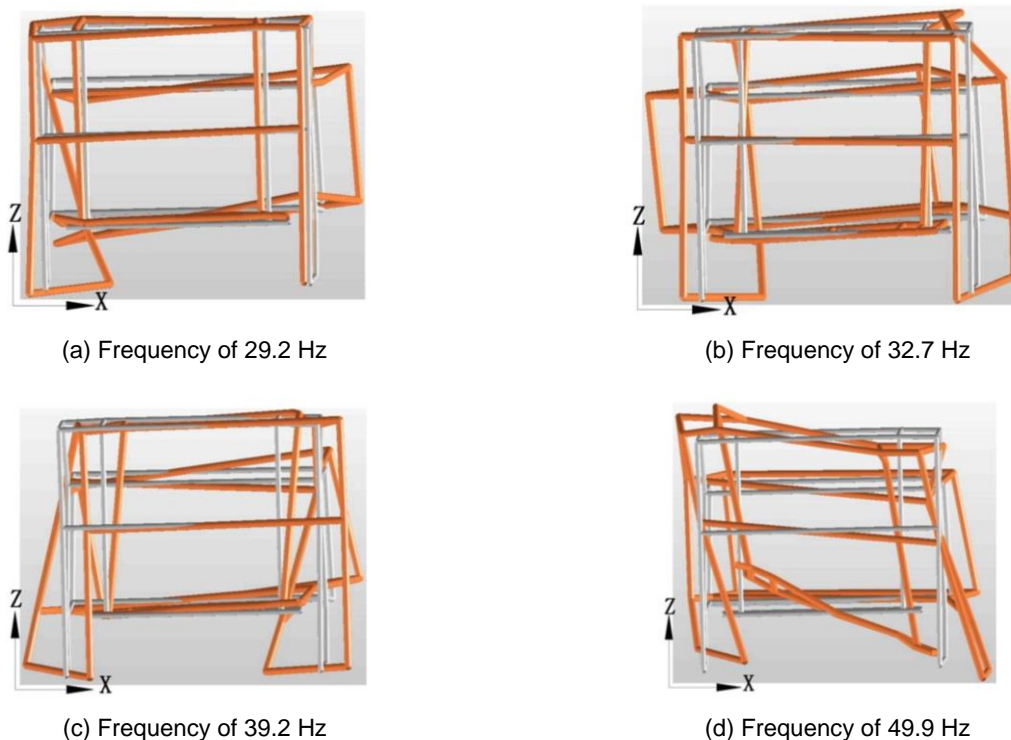


Fig. 14 - Vibration modes of optimized frame structure

It can be seen from the test results (Fig.14) that the vertical vibration mode of the optimized frame disappears, indicating that the vertical stiffness of the frame structure has been enhanced.

Figure 15 shows the vertical FRFs along different vibration transmission paths tested for the optimized frame. The frequency-response characteristics under multiple operating conditions can be extracted from it. In comparison, the response amplitude RMS ( $2.3 \text{ e}^{-3}\text{g}\cdot\text{N}^{-1}$ ) excited by the road spectrum was larger than that ( $2.2 \text{ e}^{-3}\text{g}\cdot\text{N}^{-1}$ ) of the engine. Among the two excitation sources, road excitation was the dominant factor. The peak value of frequency of excited by the road spectrum was close to the engine excitation frequency, which may cause dangerous resonance. The test results of the optimized frame were shown in Table 5. The response amplitude RMS excited by the road spectrum and engine were decreased by 21.7% and 27.2% respectively. In addition, the excitation frequencies that can produce significant amplitudes avoided two operating frequency ranges, i.e. 1~5 Hz for the road spectrum and 50~66.7 Hz for the engine.

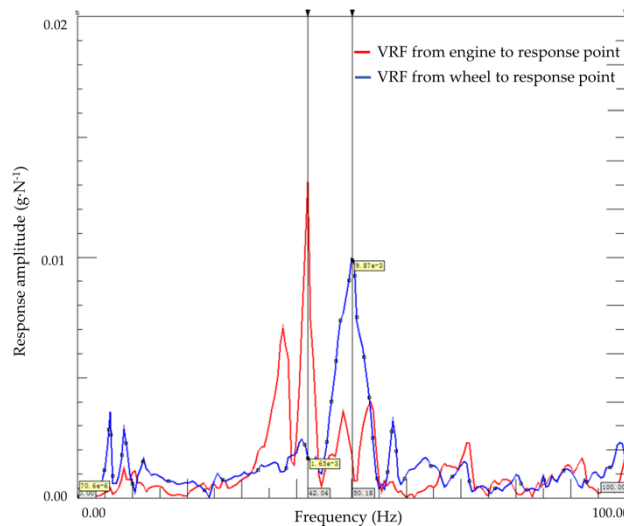


Fig. 15 - Tested frequency-response functions

Table 5 summarizes the comparison results extracted from the measured FRFs before and after frame optimization. It was found that bending and torsional stiffness of the optimized frame increased slightly, and throughout the range of 0~100 Hz, the amplitude RMS and variance values from the engine or road to the response point ( $P_e$  &  $P_r$ ) were reduced to varying degrees (21.7%~46.6%), indicating that the response characteristics of these transmission paths have been improved and the system robustness has become more stable. It was comprehensively verified that the frame achieved dynamic characteristics optimization through topological and implicit parameter optimization processes. Moreover, the vertical vibration amplitude and VI output at the cutter position were ultimately reduced by 35.9% and 5.9% respectively. Based on the positive correlation between vibration response and cutting damage, the improvements of these two indicators were obviously beneficial to reducing the cutting damage level of sugarcane.

Table 5

Comparison of VRF index before and after frame optimization

FRF Index	Initial value	Optimized value	Rate of change
Bending stiffness ( $\text{kN}\cdot\text{mm}^{-1}$ )	11.80	12.03	1.95%
Torsional stiffness [ $\text{kN}\cdot\text{m}\cdot(\text{°})^{-1}$ ]	11.98	12.32	2.84%
RMS of $P_e$ ( $\text{e}^{-3}\text{g}\cdot\text{N}^{-1}$ )	2.2	1.6	-27.2%
Variance of $P_e$ ( $\text{e}^{-6}\text{g}^2\cdot\text{N}^{-1}$ )	3.2	2.2	-31.3%
RMS of $P_r$ ( $\text{e}^{-3}\text{g}\cdot\text{N}^{-1}$ )	2.3	1.8	-21.7%
Variance of $P_r$ ( $\text{e}^{-6}\text{g}^2\cdot\text{N}^{-1}$ )	3.0	1.6	-46.6%
Vertical amplitude (mm)	0.64	0.41	-35.9%
$V_l$ ( $\text{mm}\cdot\text{s}^{-1}$ )	101.2	95.2	-5.9%

**CONCLUSIONS**

(1) This paper presented a method for optimizing cutting damage of cane stalk based on implicit parametric modeling of frame. The excitation sources under the working conditions of sugarcane harvester were analyzed qualitatively and quantitatively by combining theory and experiment. Based on the analysis of the damage mechanism of sugarcane cutting, vibration amplitude and impact velocity were proposed as dynamic indicators to characterize damage inducibility.

(2) Through the constructed dynamic model and rigid-flexible coupled virtual prototype model, the parameters with the greatest influence on the nonlinear cutter response were selected from 21 dynamic parameters by correlation analysis. The results showed that the frame stiffness and mass had the greatest correlation with responses, which pointed out the target for subsequent optimization.

(3) Combined with topological and implicit parametric optimization, the dynamic characteristics of the frame were improved. Comparison of testing results before and after optimization showed that the bending and torsional stiffness were increased by 1.95% and 2.84%, and a dangerous natural frequency was moved out of the engine's operating frequency band. The RMS of FRFs with road and engine as path sources were reduced by 21.7% and 27.2% respectively, which comprehensively improved the frequency-response characteristics of such vibration system. Finally, the output amplitude RMS and impact velocity were decreased by 35.9% and 5.9% respectively, which was beneficial to reduce the level of damage to cane stalks. This study provided a reference for the development of harvester dynamic systems based on harvesting quality optimization.

## ACKNOWLEDGEMENT

This research was funded by the Chinese Postdoctoral Science Foundation (Grant No. 2023MD734147), the Guangxi Major Science and Technology Special Project (Grant No. Guike AA22117004-1) and the Project of Guangxi Key Laboratory of Environmental Pollution Control and Ecological Restoration Technology (23-026-14).

## REFERENCES

- [1] Chen X., Hu C., Ning, H., Wu Y., Wang S., Yang C. (2016). Implicit parameterization modeling and multi-performance lightweight optimization for SUV body-in-white (SUV 白车身隐式参数化建模及多性能优化轻量化), *Journal of Jilin University (Engineering and Technology Edition)*, vol.46, no.6, pp.1780-1785.
- [2] Gupta C P., Oduori M F. (1992). Design of the Revolving Knife-Type Sugarcane Basecutter, *Transactions of the ASAE*, vol.35, no.6, pp.1747-1752.
- [3] Fan Z., Li S., Ma F., Li W., Lai X., Xue B. (2012). Simulation analysis and experiment on influence of road spectrum of cane field on cutting quality (甘蔗地路谱对切割质量影响的仿真分析与试验), *Transactions of the Chinese Society of Agricultural Engineering*, vol.28, no.1, pp.37-41.
- [4] Gu D., Ding H., Qu Y., Zhang X., Shen H., Sun S., Hu A. (2013). Development of high-speed light diesel engine for forklift (叉车用轻型高速柴油机的开发), *Chinese Internal Combustion Engine Engineering*, vol.34, no.4, pp.83-91.
- [5] Han H., Sorokin V., Tang L., Cao D. (2022). Lightweight origami isolators with deployable mechanism and quasi zero stiffness property, *Aerospace Science and Technology*, vol.121, DOI: <https://doi.org/10.1016/j.ast.2021.107319>.
- [6] Hou J., Xu W., Wang J., Chen J., Zhang K., Li Y. (2021). Analysis of vehicle-bridge coupling vibration considering the influence of expansion joint (考虑伸缩缝参数影响的连续梁桥车-桥耦合动力响应研究), *Journal of Vibration and Shock*, vol.40, no.22, pp.151-160.
- [7] Kroes S., Harris H D. (1995). A kinematic model of the dual base cutter of a sugar cane harvester, *Journal of agricultural engineering research*, vol.62, no.3, pp.163-172.
- [8] Kroes S., Harris H D. (1996). Measuring and predicting force, energy, bending strength and splitting of sugar cane during an impact cut, *In: Z. EurAgEng' 96, Madrid*.
- [9] Li S., Chen Z., Zhou J., Mo H., Zhong J. (2017). Topological optimization design of sugarcane harvester cutter based on dynamic characteristics (基于动态特性的甘蔗收获机切割器拓扑优化设计), *Journal of Agricultural Mechanization Research*, vol.39, no.9, pp.25-30.
- [10] Liu F., Yang X., Fang X., Liu Y., Wu J., Zhao J. (2018). Design and experiment of chopper device in sugarcane harvester (甘蔗收获机切段装置设计与试验), *Transactions of the Chinese Society for Agricultural Machinery*, vol.49, no.9, pp.90-94.
- [11] Liu J., Luo L., Xiao X., Zhang C., Mi C. (2022). Multi-objectives topology optimization of frame in an electric mining dump truck based on fuzzy satisfaction variable weight coefficients method, *Journal of Mechanical Science and Technology*, vol.36, pp.3059-3069, DOI: 10.1007/s12206-022-0536-5.

- [12] Liu Q., Qu Y., Qin S., Huang S. (2007). High-speed photography analysis on the damage process in cutting sugarcane stalk with smooth edge blade (光刃刀片切割甘蔗茎秆破坏过程高速摄像分析), *Transactions of the Chinese Society for Agricultural Machinery*, vol.38, no.10, pp.31-35.
- [13] Liu Q., Qu Y., Qin S., Song C. (2007). Cutting force test of sugarcane stalk (甘蔗茎秆切割力试验), *Transactions of the Chinese Society of Agricultural Engineering*, vol.23, no.7, pp.90-94.
- [14] Lv Y., Yang J., Liang Z., Mo J., Qiao Y. (2008). Simulative kinematics analysis on the affecting factors of rate of broken biennial root of single base cutter of sugarcane harvester (单圆盘甘蔗切割器影响破头率的运动学仿真), *Transactions of the Chinese Society for Agricultural Machinery*, vol.6, no.4, pp.50-55.
- [15] Ma F., He Y., Li S., Liang S., Hu S. (2006). Analysis on fuzzy comprehensive evaluation and optimization of cutting performance of sugarcane harvester (甘蔗收获机切割性能的模糊综合评价与优化), *Transactions of the Chinese Society for Agricultural Machinery*, vol.37, no.12, pp.79-82.
- [16] Marin E., Cârdei P., Vlăduț V., Biriș S-Șt., Ungureanu N., Bungescu S.T., Voicea I., Cujbescu D., Găgeanu I., Popa L-D., Isitcioaia S., Matei Gh., Boruz S., Teliban G., Radu C., Kabas O., Caba I., Maciej J. (2023). Research on the influence of the main vibration-generating components in grain harvesters on the operator's comfort, *INMATEH – Agricultural Engineering* 74 (3), pp. 800-815, DOI: <https://doi.org/10.35633/inmateh-74-85>.
- [17] Mello, R. D. C., & Harris, H. (2001). Angled and serrated blades reduce damage, force and energy for a harvester basecutter. *Proc. Conf. Australian Soc. Sugar Cane Tech.* pp. 1212-1218.
- [18] Mo H., Qiu C., Li S., Ma S. (2022). Dynamic characteristic research on a simulated sugarcane field exciter for small sugarcane harvesters: simulations and experiments, *Journal of Vibroengineering*, vol.24, no.5, pp.806-823, DOI:10.21595/jve.2022.22015.
- [19] Mo J., Liu Q. (2013). Discussion on the mechanization technology of sugarcane harvesting in China (我国甘蔗收获机械化技术探讨), *Journal of Agricultural Mechanization Research*, vol.35, no.3, pp.12-18.
- [20] Momin M A., Wempe P A., Grift T E., Hansen A. (2017). Effects of Four Base Cutter Blade Designs on Sugarcane Stem Cut Quality, *Transactions of the ASABE*, vol.60, pp.1551-1560.
- [21] Pelloso M., Pelloso B F., de Lima A A., Ortiz A. (2021). Influence of harvester and rotation of the primary extractor speed in the agroindustrial performance of sugarcane, *Sugar Tech*, vol.23, pp.692-696, DOI: <https://doi.org/10.1007/s12355-020-00944-6>.
- [22] Razavi J., Kardany M., Masoumi A. (2010). Effects of some cutting blades and plant factors on specific cutting energy of sugarcane stalk. *17th World Congress of the International Commission of Agricultural Engineering (CIGR)*. Québec City, Canada June 13-17, 2010
- [23] Silva., Rouverson & Corrêa., Caio & Cortez. (2008). Statistical control applied in the process of mechanical sugar cane harvest. *Engenharia Agrícola*, vol.28, no.2, pp.292-304.
- [24] Vlăduț V., Biriș S.Șt., Bungescu T., Herișanu N. (2013). The influence of vibrations on the operator in the grain harvesters, *Applied Mechanics and Materials*, Vol. 430, pp 290-296, DOI: 10.4028/www.scientific.net/AMM.430.290.
- [25] Wang F., Zhang W., Di M., Wu X., Song Z., Xie B., Yang G., Ma S. (2019). Sugarcane Cutting Quality Using Contra-Rotating Basecutters, *Transactions of the ASABE*, vol.62, no.3, pp.737-747, DOI: 10.13031/trans.12716.
- [26] Wu J., Chen R., Qiu L., Fan Y., Li Y., Deng Y., Yan H., Zhou H., Zhou Z., Li A. (2022). Study on the effect of different reseeding methods on sugarcane (不同补种方法对宿根蔗的效果研究), *Sugarcane and Canesugar*, vol.51, no.4, pp.7-12.
- [27] Xu N., Ren Z., Li X., Cha H. (2017). Study on vertical vibration transmission and ride performance with the coupling effect between vehicle and suspended devices (车辆与吊挂设备耦合作用垂向系统振动传递及平稳性研究), *Journal of Vibration Engineering*, vol.30, no.6, pp.965-975.
- [28] Yan G., Shen X., Yu F., Zhu B., Liang W. (2020). Optimization design of frame structure of ROV based on ANSYS-Workbench (基于 ANSYS-Workbench 对水下机器人框架结构优化设计), *Manufacturing Automation*, vol.42, no.10, pp. 1-3+7.
- [29] Yang R., Zhou H., Liang Q., Tang S., Wang L., Gui Y., Huang H., Huang Z., Xian W., Lei J. (2021). Analysis of ratoon ability for sugarcane families (甘蔗家系宿根性分析), *Chinese Journal of Tropical Crops*, vol.42, no.7, pp.1932-1940.

- [30] Yang W., Wang E., Yang J., Li Y., Huang S., Liang Z. (2017). Test of the factors influencing the cutting quality of Case A8000 sugarcane combine (凯斯 A8000 甘蔗联合收割机切割质量影响因素的试验), *Journal of Agricultural Mechanization Research*, vol.39, no.5, pp.192-196.
- [31] Zou Z., Wu T., Gao Z., Zhang Z., Liu Q. (2018). Design and test of cut-off auto control system for sugarcane billet harvester (甘蔗收割机切割刀盘浮动控制系统的设计与试验), *Journal of Henan Agricultural University*, vol.52, no.1, pp.73-79.
- [32] Zhang Q., Xian Y., Xiao Q., Xu L., Li Z., Yi S., Li L. (2023). Backstepping sliding mode control strategy of non-contact 6-DOF Lorentz force platform, *Journal of Vibration and Control*, vol.29, no.5-6, pp.1061-1075.
- [33] Zhou J., Li S., Yang D., Zhong J., Mo H., Zhang B., Deng X. (2017). Influence of sugarcane harvester cutterhead axial vibration on sugarcane ratoon cutting quality (甘蔗收获机刀盘轴向振动对甘蔗宿根切割质量的影响), *Transactions of the Chinese Society of Agricultural Engineering*, vol.33, no.2, pp.16-24.
- [34] Zhou J., Li S., Mo H. (2018). Test on influence of sugarcane harvester's dynamic properties on the broken rate of ratoons (甘蔗收获机动态特性对宿根破头率影响的试验), *Journal of Agricultural Mechanization Research*, vol.40, no.2, pp.150-156.